PERGAMON

International Journal of Heat and Mass Transfer 45 (2002) 3357–3368

International Journal of HEAT and MASS TRANSFER

www.elsevier.com/locate/ijhmt

Visualization of mixed convective vortex rolls in an impinging jet flow of air through a cylindrical chamber

T.C. Cheng, P.H. Chiou, T.F. Lin *

Department of Mechanical Engineering, National Chiao Tung University, Hsinchu 30010, Taiwan, ROC

Received 20 October 2000; received in revised form 11 January 2002

Abstract

In this study a combined buoyancy and inertia driven vortex flow in an air jet impinging onto a heated circular plate confined in a cylindrical chamber simulating that in a vertical single-wafer rapid thermal processor for semiconductor manufacturing is investigated experimentally by flow visualization. A copper plate is used here to simulate the wafer for its better uniformity of the surface temperature and air is used to replace the inert gases. We concentrate on how the inlet gas flow rate, temperature difference between the wafer and air jet, and chamber pressure affect the vortex flow. The results show that typically the flow in the chamber is in the form of two-roll structure characterized by a circular vortex roll around the air jet along with another circular roll near the side wall of the chamber. Both rolls are somewhat deformed. The rolls are generated by the reflection of the jet from the wafer and by the deflection of the wall boundary layer flow along the wafer surface by the upward buoyancy due to the heated wafer. At low buoyancy and inertia the vortex rolls are steady and axisymmetric. At increasing buoyancy associated with the higher temperature difference and chamber pressure, the inner roll becomes slightly smaller and the outer roll becomes correspondingly bigger. Moreover, at a higher gas flow rate the inner roll is substantially bigger. Based on the present data, a correlation equation is provided to predict the location where the two rolls contact each other, providing the approximate size of the rolls. Moreover, at high buoyancy and inertia the flow becomes time dependent and does not evolve to a steady state.

1. Introduction

The vortex flow induced by a round gas jet impinging onto a circular heated disk in a confined cylindrical chamber is frequently encountered in various technological processes such as cooling of microelectronic equipments [1], growth of thin crystal films in vertical chemical vapor deposition (CVD) reactors [2], and fabrication of ultra large scale integrated (ULSI) circuits through the single-wafer rapid thermal processes (RTP) [3]. Apparently, the structure of the vortex flow is mainly affected by the inertia of the jet, buoyancy force due to the hot disk, and geometry of the chamber including the jet diameter, jet-to-disk distance, disk and chamber diameters. But, the details on how these relevant parameters affect the vortex flow characteristics remain largely unexplored. In the present study experimental flow visualization is conducted to investigate the vortex flow patterns driven by the inertia and buoyancy in the confined impinging gas jet flow. Particular attention is paid to simulating the vortex flow normally seen in vertical single-wafer RTP processors.

In what follows the relevant literature on the present study is briefly reviewed. Considerable amount of work from a number of research groups has been carried out in the past to study the fluid flow and heat transfer in the round or slot jet impinging onto a large horizontal plate. Most of the studies focus on quantifying the highly efficient heat transfer associated with the high speed impinging jets and the jets considered have a much higher inertia than the buoyancy force generated by the temperature gradient in the flow. Therefore the jet impinging flow is dominated by the jet inertia and some

* Corresponding author. Tel.: +886-35712121-55118; fax: +886-357-26440.

E-mail address: t7217@cc.nctu.edu.tw (T.F. Lin).

0017-9310/02/$ - see front matter
PII: S0017-9310(02)00055-8

Nomenclature

D_j	diameter of jet at the pipe exit
D_{wf}	diameter of wafer
g	magnitude of gravitational acceleration
Gr	Grashof number ($\beta g \Delta T H^3/\nu^2$)
Gr/Re_j^2	buoyancy-to-inertia ratio ($\beta g \pi^2 D_j^2 \Delta T H^3/16 Q_j^2$)
H	distance from pipe exit to copper plate
L	the distance from the stagnation point of the jet impinging on the plate to the location where the flow along the wafer surface is lifted up
P	total pressure in the processor
Q_j	gas volume flow rate
Ra	Rayleigh number ($\beta g \Delta T H^3/\alpha\nu$)
Re_j	jet Reynolds number ($V_j D_j/\nu$)
t	time
t_p	period of time periodic flow
V_j	velocity of the gas jet at the pipe exit
α	thermal diffusivity
β	thermal expansion coefficient
ν	kinematic viscosity
ΔT	temperature difference between the copper plate and the ambient air

geometric parameters of the system. For instances, heat or mass transfer in the laminar and turbulent impinging jets was experimentally investigated by Gardon and Akfirat [4,5], Scholtz and Trass [6], Sparrow and Wong [7], Masliyah and Nguyen [8], and Hrycak [9]. Recently, the flow and thermal structures of the turbulent round jets were examined by Özdermir and Whitelaw [10] and Liu and Sullivan [11]. Moreover, numerical computation was performed to predict the flow and heat transfer in the laminar impinging jets with the presence of an upper plate confinement from [12–14]. Besides, the results from the computation for the turbulent impinging jets were reported by Hosseinalipour and Mujumdar [15] and Morris and Garimella [16]. The corresponding heat transfer coefficient for the confined impinging jets was measured by Lin et al. [17]. A combined experimental and numerical study was recently conducted by Incropera and his colleagues [18,19] to explore the impinging liquid jets confined by a cylindrical container. More complete information on the impinging jets can be found from the recent critical reviews by Viskanta [20] and Jambunathan et al. [21]. It should be pointed out that in the above studies [4–21] the buoyancy force exhibits negligible effects on the jet flow.

In the impinging jet flow encountered in the CVD and RTP processes, the gases input to the CVD reactors and RTP processors are at relatively low flow rates and the silicon wafer upon which semiconductor thin crystal films are grown and processed is at an elevated temperature. Under such circumstance the buoyancy in the flow is no longer small compared with the jet inertia. Significant flow recirculation can be induced by the buoyancy and the impinging jet flow is driven by the combined effects of the inertia and buoyancy. The importance of the buoyancy on the recirculating flow in a vertical CVD reactor was demonstrated by Wahl [22]. Similar investigations have been carried out for various types of CVD reactors including the metal organic CVD [23–27] and single-wafer RTP processors [28–30]. In these studies for the processing of the microelectronic circuits [22–30] various vortex flow patterns were reported in the jet impinging flow.

The above literature review clearly reveals that the detailed vortex flow characteristics associated with a mixed convective low speed round gas jet impinging onto a heated circular plate in a confined chamber are still poorly understood. In this study an experimental system is established to observe the vortex flow patterns in this confined impinging jet flow. Attention is focused on how the jet flow rate, temperature difference between the plate and jet, and chamber pressure affect the vortex flow patterns.

2. Experimental apparatus and procedures

In order to conduct the experiment at reasonably low cost, we use air as the working fluid to replace the inert gases normally employed in real RTP. In view of the similar thermodynamic and thermophysical properties for various gases, the results obtained here are still applicable to the RTP systems. The major parts in the system are briefly described in the following. The experimental system established in the present study to investigate the mixed convective vortex flow patterns resulting from a low speed round air jet impinging onto a circular heated disk in a cylindrical chamber, simulating the flow in a vertical single-wafer RTP processor, is schematically shown in Fig. 1. The system consists of six major parts – the processing chamber, temperature measurement and data acquisition unit, heating lamp unit, gas injection unit, vacuum unit, and control unit. The air drawn from the ambient is compressed into a connection pipe and regulated by a pressure regulator. Then the air is passed through several filters to remove the possible presence of oil, moisture and particles in it. Besides, the air pressure, flow rate and temperature are measured. Finally, the air is brought into the processing

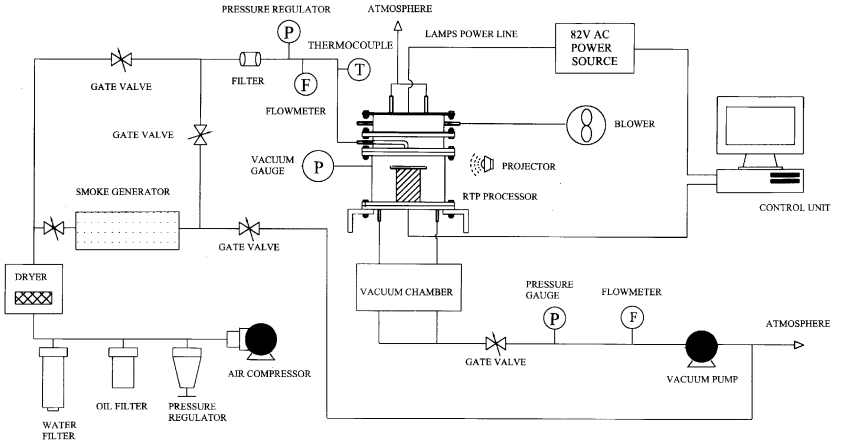

Fig. 1. Schematic diagram of the experimental apparatus.

chamber through a single-inlet pipe and then injected directly onto a circular heated disk. A vacuum pump connected to the bottom of the chamber is used to suck the gas out of the chamber (Fig. 2).

The processing chamber is cylindrical and has a diameter of 30 cm. Its side wall is made of 6 mm thick quartz glass to allow for the observation of the flow pattern in the chamber. The entire chamber is insulated

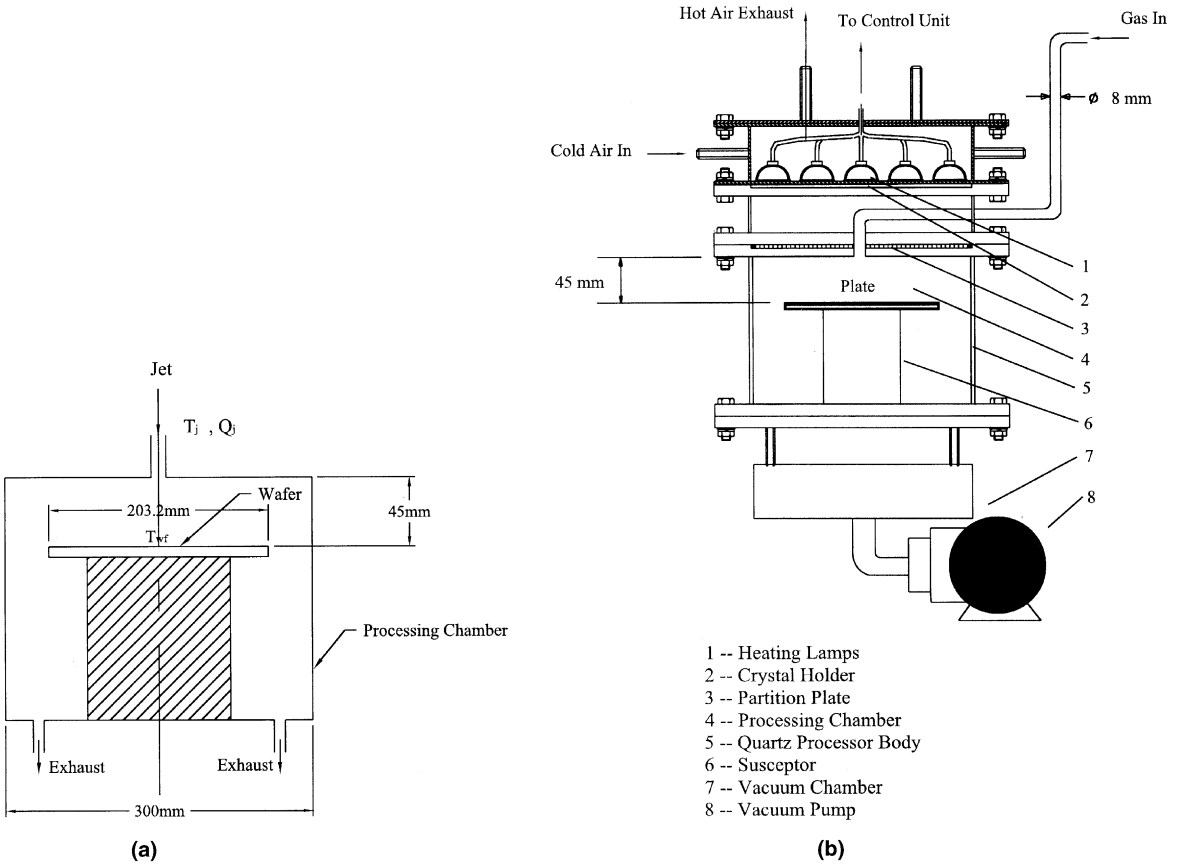

Fig. 2. Schematic of the test section (processing chamber) (a) and cross-sectional view of the main part of the experimental system (b).

with a superlon insulator layer of 10 cm thick. The insulator can be opened during the flow visualization experiment. We use a 1 cm thick circular copper plate having a diameter of 20 cm to simulate an 8-inch wafer. In view of the high thermal conductivity of the copper plate a nearly isothermal boundary condition on the disk surface can be obtained without very precise control of the heating lamp unit. The copper plate is fixed on a bakelite susceptor and is leveled horizontally. Eight T-type thermocouples are stuck on the back surface of the copper plate at selected locations to measure the temperature variations over the copper plate. These thermocouples are positioned at three concentric circles at an equal radial interval of 3.4 cm. Two 16-channel recorders combined with an industrial personal computer (ADVENTECH 600 series) are employed to acquire and process the data from various transducers.

To simulate the flow in a RTP system, the copper plate is heated by lamps. The lamp-heating unit consists of thirteen lamps, an AC power supply and cooling fans. The thermal radiative energy from the lamps is transmitted to the copper plate through a quartz window. More specifically, the thirteen 410 W & 82 V OSRAM tungsten–halogen lamps (with reflector) are arranged into an inner ring of four lamps and an outer ring of nine lamps. The input power to each lamp zone can be automatically adjusted in real time using two variable resistance circuits for optimal wafer temperature uniformity. To control the input power to the lamps, an ON/OFF control algorithm is used here. This algorithm is found to result in a reasonably small temporal fluctuation of the wafer temperature. We also find that the maximum temperature nonuniformity across the wafer deviating from the average wafer temperature is about ± 0.3 °C for ΔT set at 20 °C for $H = 4.5$ cm, $Q_j = 4$ slpm (standard liter per minute) and $P = 760$ Torr.

In the present study, the gas injection unit includes a 2 HP air compressor, a flow meter, a manual flow control valve, a filter, a pressure regulator and a connection pipe. The pressure regulator and flow meter are used to control the air flow rate. The downward vertical air jet issuing from the pipe exit impinges directly onto the copper plate. To pump out the processed gas and to keep the processing chamber at the preset pressure, a rotary vacuum pump (SINKU KIKO GCD-050) with a 200 slpm pumping capacity is installed in the system. The pumping rate can be adjusted by the manual flow control valve and the gas leaving the processing chamber is sucked out to an exhaust gas treating unit. The system pressure of the chamber is maintained at the required level by adjusting the flow rate of the vacuum pump.

To visualize the vortex flow in the processing chamber, a smoke generator is installed in the experimental system to add smoke to the inlet air. The smoke comes from burning the incense prepared from sandalwood. The smoke is mixed uniformly in the smoke generator and is carried out by the inlet air and sent into the processing chamber. A vertical plane light sheet shines through the flow field containing the tiny incense particles. The thin plane light sheet is produced by two razor blades and a YOKOGAWA xenon slide projector. The Nikon FM2 camera with the max diaphragm of 1.4 and suitable exposure time, varying from 1/60 to 1/4 s, is used to picture the flow patterns from the chamber side. Besides, a digital video camera (Sony PC-100) also takes the consecutive pictures of the time dependent flow patterns.

Table 1
Summary of uncertainty analysis

Parameters	Uncertainty
D_j, D_{wf}, H (m)	± 0.00005 m
P (Torr)	± 1 Torr
ΔT	± 0.4 °C
μ (Nm/s^2)	$\pm 0.05\%$
α (m^2/s)	$\pm 0.07\%$
ν (m^2/s)	$\pm 0.07\%$
V_j (m/s)	$\pm 1.4\%$
Q_j (L/min)	$\pm 1.5\%$
Ra	$\pm 10.5\%$
Re_j	$\pm 2.26\%$

For each case the experiment starts with the air at the room temperature T_a compressed first into a smoke generator through the connection pipe and then injected into the processing chamber. The air moves over the wafer and finally is sucked out of the processing chamber through the exhaust ports. In the meantime the temperature of wafer and the chamber pressure are controlled at the preset levels. As the air flow in the processing chamber reaches steady or statistically stable state, we begin to visualize the vortex flow pattern in the chamber.

An uncertainty analysis based on the procedures proposed by Kline and McClintock [31] was carried out here to estimate the uncertainty levels in the experiment. The results from this uncertainty analysis are summarized in Table 1.

3. Results and discussion

As mentioned above, the mixed convective vortex flow in the experimental system under investigation is affected by the chamber pressure P, gas flow rate entering the processor Q_j, wafer-to-ambient air temperature difference ΔT, and the distance between the connection pipe exit and copper plate H. The present experiments are carried out to explore the effects of the gas flow rate, jet-to-wafer temperature difference, and chamber pressure on the vortex flow pattern for H fixed at 4.5 cm. In particular, Q_j is varied from 0.5 to 5.0 slpm,

ΔT is varied from 0 to 20 °C, and P is varied from 300 to 760 Torr. In what follows selected flow photos taken in the present study are examined in detail to unravel the gas flow patterns resulting from the air impinging jet in the processing chamber.

3.1. Typical flow pattern

At first, the typical flow pattern observed in the processing chamber at steady or statistically stable state is illustrated in Fig. 3 in which the steady side view flow photo along with the corresponding schematic sketch of the flow based on the detailed flow visualization for $P = 450$ Torr, $Q_j = 3.0$ slpm and $\Delta T = 10$ °C is shown. For this typical case the Reynolds number of the air jet based on the jet diameter and speed at the pipe exit is 520.1. Thus we have a laminar impinging jet issuing from the pipe [20]. The result for this cross-plane recirculating flow viewing from the chamber side indicates that as the downward air jet hits the copper plate, it is deflected immediately and moves radially outward along the plate surface. It is of interest to note that due to radial spread of the impinging jet, the wall flow slows down quickly as it travels downstream. Then, in a short distance the air flow along the plate surface is slow enough and is lifted up to move vertically by the upward buoyancy generated by the heated copper plate. The upmoving air flow later is retarded by the upper horizontal wall of the processing chamber and is drawn towards the inner zone of the chamber surrounding the downward jet in which a low pressure region is created by the air jet. Before hitting the jet, it turns to move vertically upwards and then moves radially outward as the flow encounters the top wall of the chamber. Note that during the above flow development a circular roll directly surrounding the air jet is induced by the buoyancy in the inner region of the chamber right above the wafer. Meanwhile, another circular roll is also induced by the buoyancy in the outer region of the chamber. Besides, a comparatively smaller and weaker circular roll appears above the inner roll and near the top wall. It also needs to be pointed out that the resulting recirculating flow is axisymmetric although the cross-sections of the rolls are somewhat deformed. The above result clearly suggests that the typical vortex flow in the chamber is dominated by the two-roll structure.

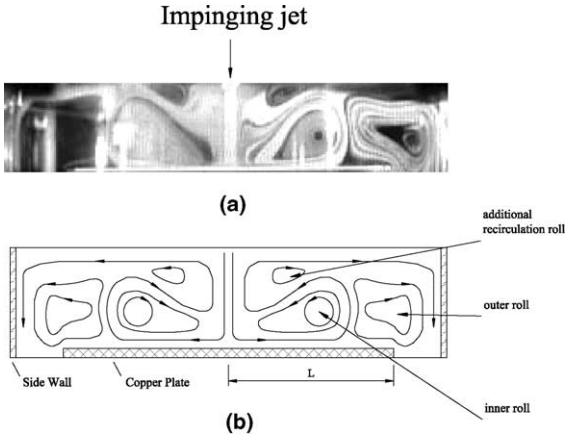

Fig. 3. Steady flow pattern viewing from the chamber side at $P = 450$ Torr, $\Delta T = 10$ °C ($Ra = 24938.9$) and $Q_j = 3.0$ slpm ($Re_j = 520.1$): (a) the photograph; (b) the corresponding schematically sketched vortex flow.

3.2. Effects of jet flow rate

How the change in the flow rate of the impinging jet affects the gas flow pattern at long time in the processing chamber is manifested in Figs. 4 and 5 by presenting the flow photos for $Q_j = 0.5$, 1.0, 2.0, 3.0 and 4.0 slpm ($Re_j = 86.6$, 173.3, 246.7, 520.1 and 693.4) at selected ΔT and P. Note that the two bright vertical broad lines in each photo are the reflection of the plane light sheet used for flow visualization on the cylindrical chamber wall and they have no connection with the vortex flow patterns. The results in these figures indicate that at given ΔT and P an increase in the jet flow rate causes the jet inertia to rise and hence the buoyancy-to-inertia ratio to become lower. Accordingly, the jet flow after impinging the copper plate travels a longer distance along the plate surface before it is lifted up by the buoyancy for a higher Q_j, resulting in a bigger inner roll and the outer roll is squeezed to become smaller. Besides, a close inspection of these flow photos further reveals that the small and weak roll near the top wall of the chamber mentioned previously does not exist at low jet flow rates for $Q_j = 0.5$ & 1.0 slpm. This is the direct consequence of the fact that at the low jet flow rate the inner roll is small and the outer roll is rather large. Thus, the space above the inner roll is not large enough for an additional recirculation roll to be induced.

3.3. Effects of temperature difference between the copper plate and air jet

The effects of the temperature difference between the copper plate and the air injected into the processing chamber on the recirculating flow in the chamber are presented in Figs. 6 and 7 for ΔT ranging from 0 to 20 °C ($Ra = 0$–43169.6) at selected P and Q_j. The results in Fig. 6 for $P = 450$ Torr and $Q_j = 3$ slpm ($Re_j = 520.1$) indicate that when the copper plate is at the same temperature as the injected air for $\Delta T = 0$ °C (the unheating case), no buoyancy exists and the impinging jet flow is completely driven by the jet inertia and the chamber geometry. In such case the jet flow mainly moves radially outward along the plate surface after it impinges the plate (Fig. 6(a)). Due to the jet impingement the wall

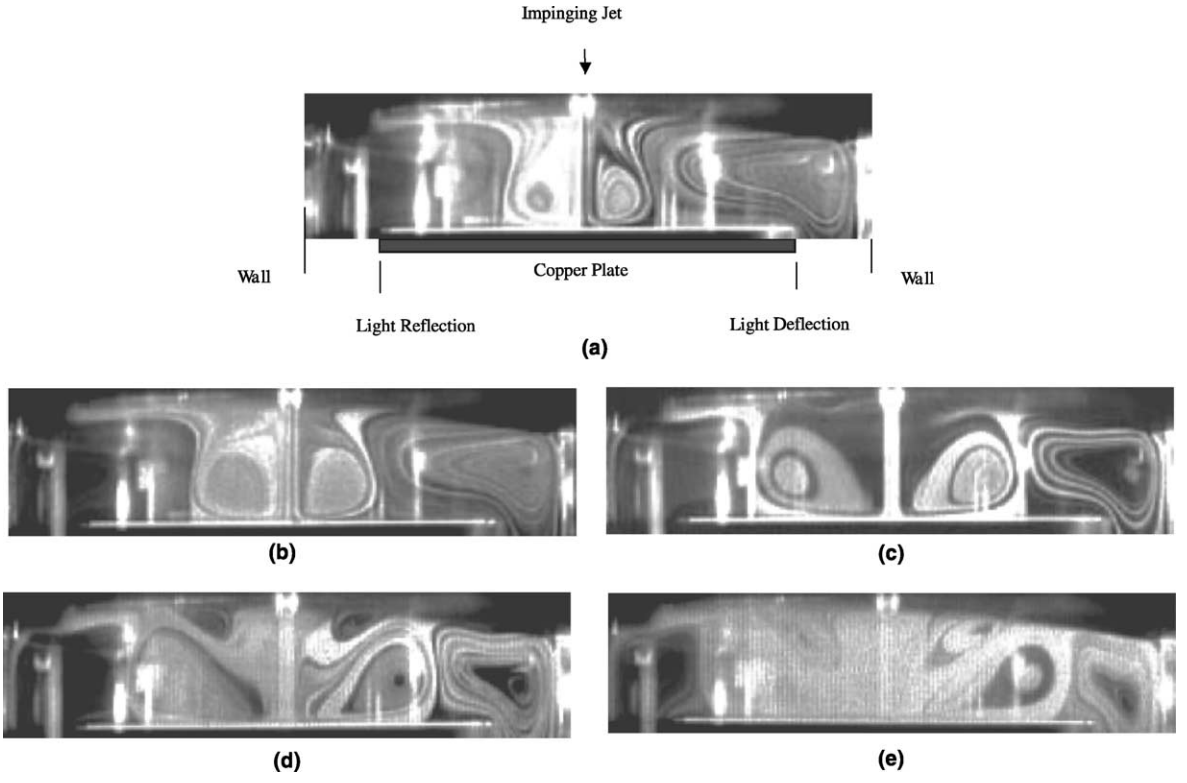

Fig. 4. Photographs of the flow pattern for $\Delta T = 10$ °C and $P = 450$ Torr ($Ra = 24938.9$) with $Q_j =$ (a) 0.5 slpm ($Re_j = 86.6$), (b) 1.0 slpm ($Re_j = 173.3$), (c) 2.0 slpm ($Re_j = 346.7$), (d) 3.0 slpm ($Re_j = 520.1$) and (e) 4.0 slpm ($Re_j = 693.4$).

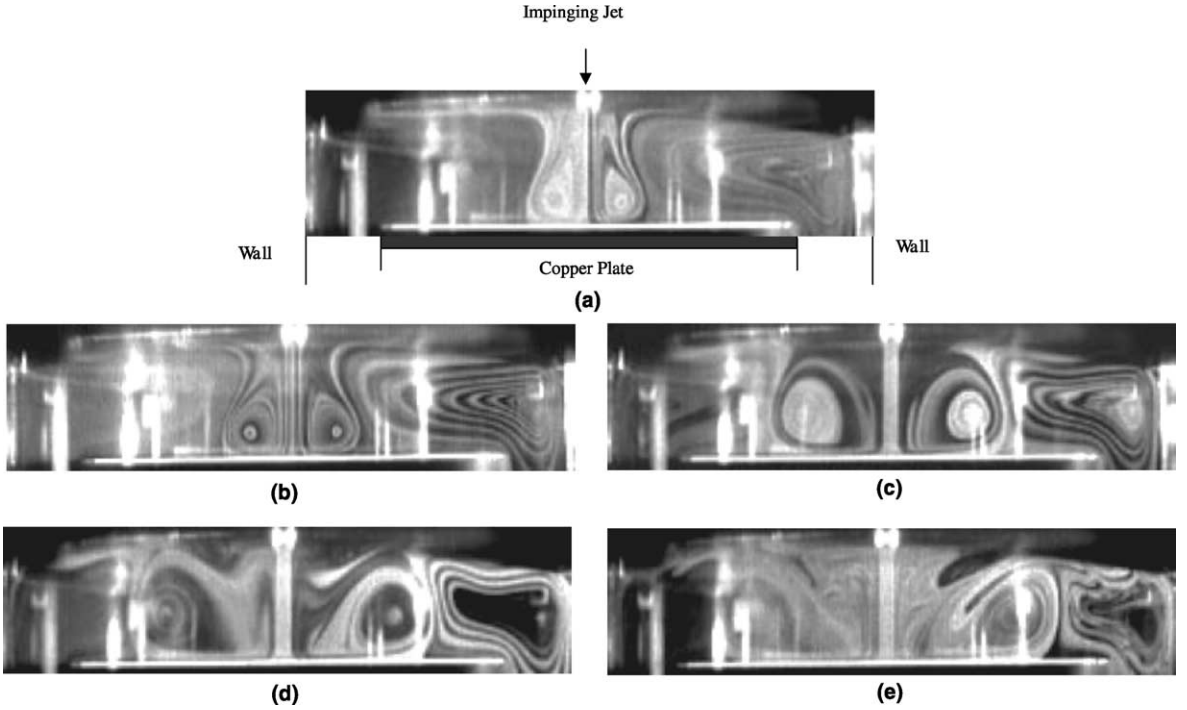

Fig. 5. Photographs of the flow pattern for $\Delta T = 15$ °C and $P = 450$ Torr ($Ra = 24775.8$) with $Q_j =$ (a) 0.5 slpm ($Re_j = 86.6$), (b) 1.0 slpm ($Re_j = 173.3$), (c) 2.0 slpm ($Re_j = 346.7$), (d) 3.0 slpm ($Re_j = 520.1$) and (e) 4.0 slpm ($Re_j = 693.4$).

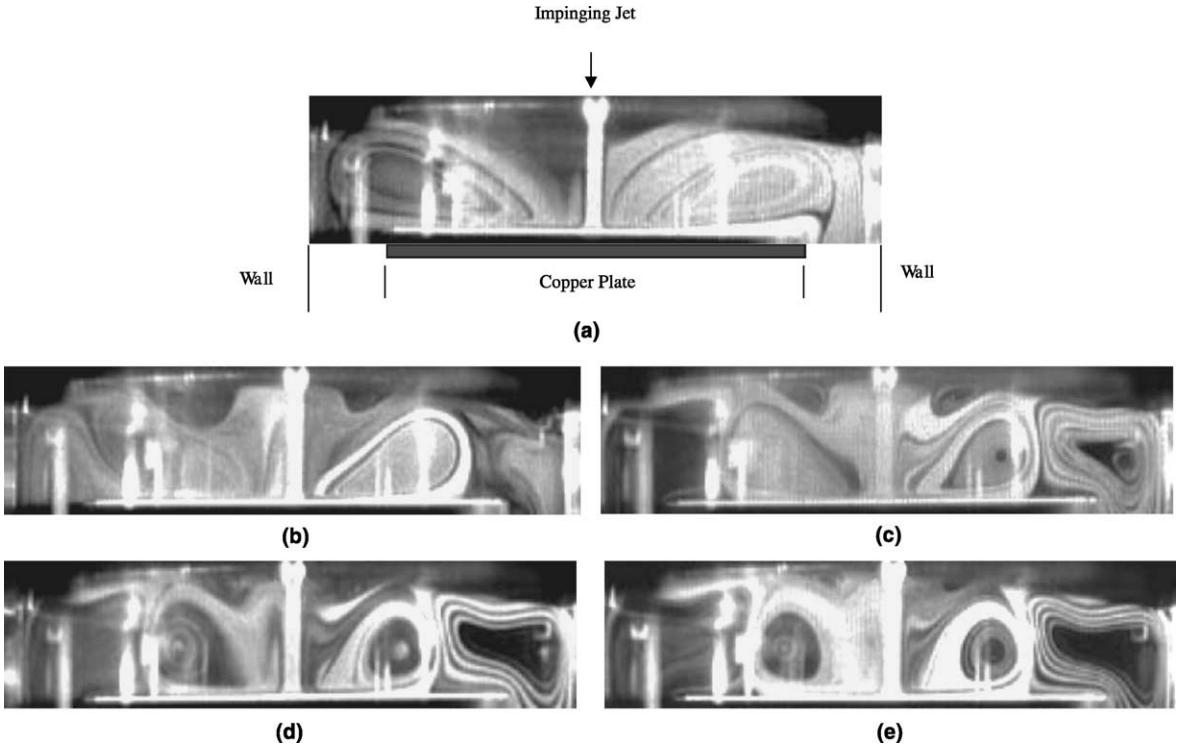

Fig. 6. Photographs of the flow pattern for $Q_j = 3.0$ slpm ($Re_j = 520.1$) and $P = 450$ Torr with $\Delta T =$ (a) 0 °C ($Ra = 0$), (b) 5 °C ($Ra = 13444.1$), (c) 10 °C ($Ra = 24938.9$), (d) 15 °C ($Ra = 34775.8$) and (e) 20 °C ($Ra = 43169.6$).

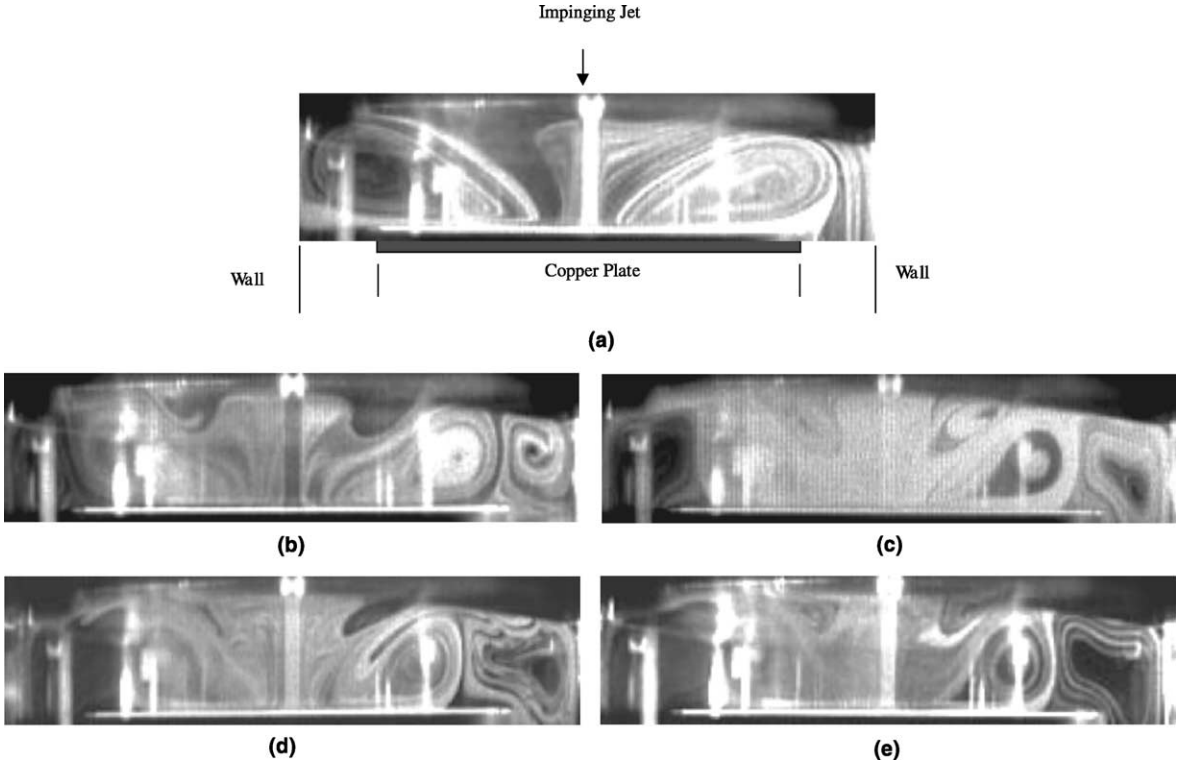

Fig. 7. Photographs of the flow pattern for $Q_j = 4.0$ slpm ($Re_j = 693.4$) and $P = 450$ Torr with $\Delta T =$ (a) 0 °C ($Ra = 0$), (b) 5 °C ($Ra = 13444.1$), (c) 10 °C ($Ra = 24938.9$), (d) 15 °C ($Ra = 34775.8$) and (e) 20 °C ($Ra = 43169.6$).

boundary layer thickens as the flow moves radially outward. As the outer portion of the wall layer hits the lateral wall of the processing chamber it is deflected and travels towards the top of the chamber. Thus, only a big circular vortex roll forms in the flow. Meanwhile, the inner portion of the wall layer moves downward as it leaves the edge of the copper plate. At the small ΔT of 5 °C the wall jet is lifted up by the small upward buoyancy to form an inner roll. Meanwhile, a small and weak outer circular roll is induced by the buoyancy (Fig. 6(b)). For a rise of ΔT to 10 °C, 15 °C or 20 °C both the inner and outer rolls become stronger. Note that for ΔT raised from 10 to 20 °C, the buoyancy becomes double but the inner roll is only slightly smaller, signifying the weak effects of the buoyancy on the roll size (Figs. 6(c) and (e)). Similar trend is noted for $Q_j = 4$ slpm in Fig. 7. An overall inspection of the results in Figs. 4–7 suggests that the buoyancy exhibits strong effects on the roll size only at low gas flow rate for $Q_j = 0.5$, 1.0 & 2.0 slpm. It is also worth noting from these photos that for ΔT exceeding certain level and the flow rate larger than 3 slpm, an additional small and weak recirculation roll appears above the inner roll.

3.4. Effects of chamber pressure

Note that at a given mass flow rate of air injected into the processor and for a given imposed temperature difference between the air jet and copper plate, the Rayleigh number of the gas flow in the chamber is proportional to the square of the gas pressure [32]. Thus, lowering the chamber pressure can effectively reduce the natural convection effects and diminish the strength of the buoyancy driven recirculating flow in the chamber. This can be clearly seen from the results in Figs. 8 and 9. A close inspection of the flow photos in these figures further reveals that only at the low gas flow rate the size of the inner and outer rolls is sensitive to the pressure change (Fig. 8) especially when P is lowered from 450 to 300 Torr. Note that at the low flow rate of 0.5 slpm and at the atmospheric pressure of 760 Torr the inner roll almost disappears for a high ΔT (Fig. 8(d)). It is also noted that at the lowest flow rate tested here for $Q_j = 0.5$ slpm the jet inertia is rather small and the jet does not possess enough momentum to reach the copper plate (Fig. 8(a)).

3.5. Time dependent recirculating flow

Our flow visualization has revealed that when the jet inertia and the buoyancy from the heated copper plate exceed certain critical levels, the recirculating flow in the processing chamber becomes time dependent and no steady flow exists at long time. This is demonstrated in Fig. 10 for a time periodic case by showing the flow patterns at four selected time instants in a typical periodic cycle in the statistical state. Note that the flow path of the impinging jet changes significantly in time. Besides, the up-moving air flow swings slightly back and forth in the radial direction. Sometimes it was sucked into the inner roll and sometimes it was drawn out by the outer roll. The process repeats periodically in time. So the inner and outer rolls influence each other and their sizes change with time. But the flow is still nearly axisymmetric.

3.6. Flow regime map

Based on the present data, a flow regime map delineating the temporal state of the driven flow in the

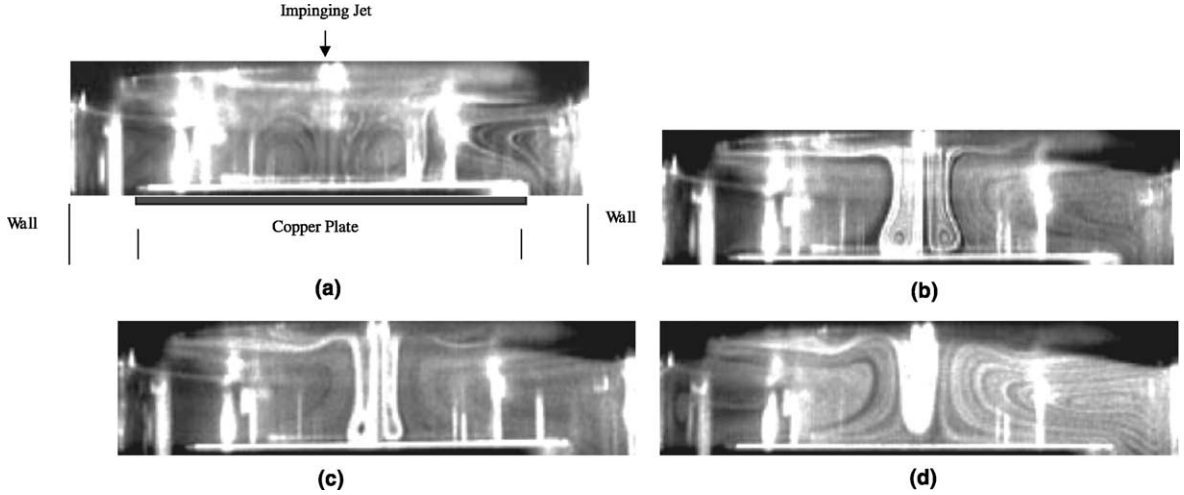

Fig. 8. Photographs of the flow pattern for $\Delta T = 20$ °C and $Q_j = 0.5$ slpm ($Re_j = 86.6$) with $P =$ (a) 300 Torr ($Ra = 19121.4$), (b) 450 Torr ($Ra = 43169.6$), (c) 600 Torr ($Ra = 76653.5$) and (d) 760 Torr ($Ra = 123165.2$).

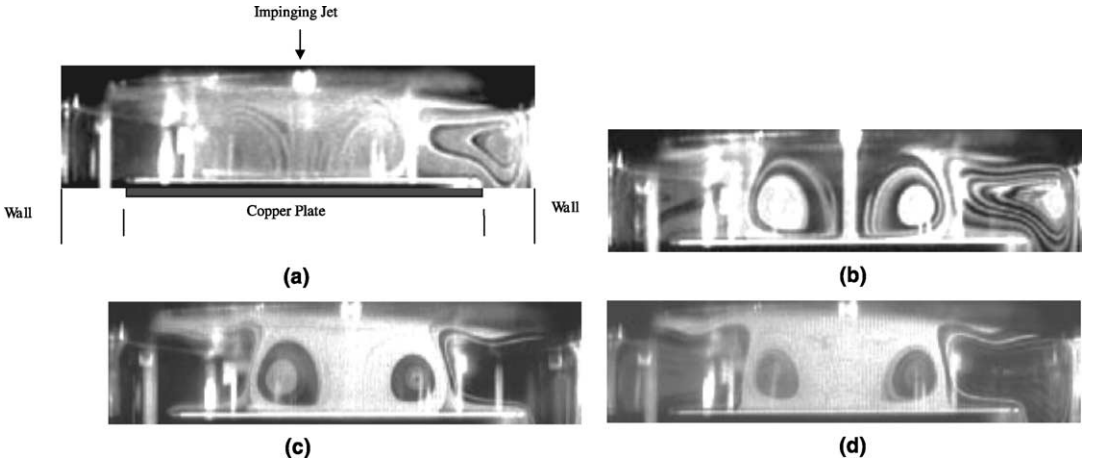

Fig. 9. Photographs of the flow pattern for $\Delta T = 15$ °C and $Q_j = 2$ slpm ($Re_j = 346.7$) with $P =$ (a) 300 Torr ($Ra = 15403.3$), (b) 450 Torr ($Ra = 34775.9$), (c) 600 Torr ($Ra = 61775.9$) and (d) 760 Torr ($Ra = 99168.0$).

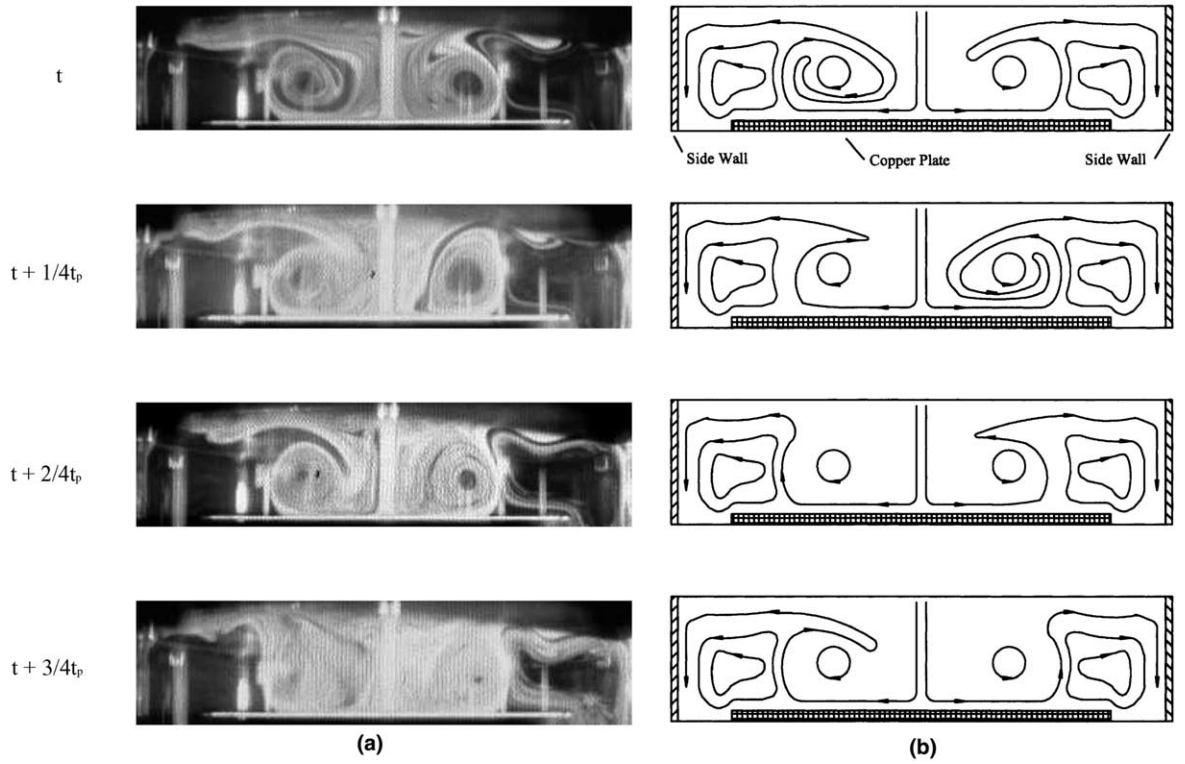

Fig. 10. (a) Photographs of the flow pattern in a typical periodic cycle for $P = 600$ Torr, $\Delta T = 20$ °C ($Ra = 76653.5$) and $Q_j = 3$ slpm ($Re_j = 520.1$) and (b) the corresponding schematically sketched flow pattern ($t_p = 2$ s).

processor in terms of Ra vs. Re_j is provided in Fig. 11. These results suggest that at the pressure of 300 and 450 Torr the buoyancy for all cases studied here is low and the driven recirculating flow all evolves to a steady state. As the pressure is raised to 600 Torr, the time periodic flow is noted for two cases with high Re_j. At an even

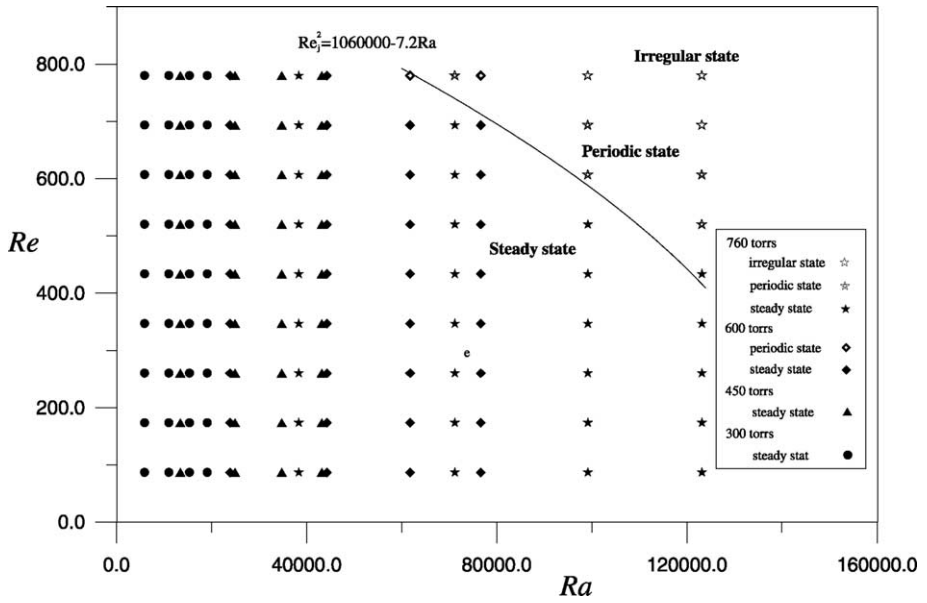

Fig. 11. The flow regime map in terms of Reynolds number versus Rayleigh number.

higher pressure of 760 Torr, flow can become time periodic and even chaotic at high Re_j and Ra. The lower bound for the time period state is correlated as

$$Re_j^2 = 1.06 \times 10^6 - 7.2Ra. \quad (1)$$

It is certainly important to understand how the Reynolds and Rayleigh numbers affect the size of the vortex rolls. We measured the distance from the stagnation point of the jet impinging on the plate to the location where the flow along the wafer surface is lifted up, L. Based on the present data, this distance can be correlated as

$$2L/D_{wf} = -1.150 + 12.15/\ln(Ra) + 0.0055Re^{0.5}\ln(Re). \quad (2)$$

The above correlation and our data are plotted in Fig. 12. The results indicate that the lift-up distance is mainly determined by the jet Reynolds number Re_j and the effect of the buoyancy is milder.

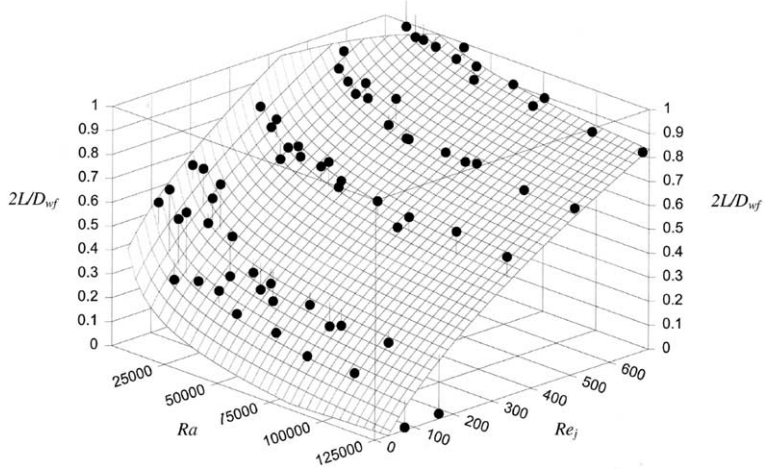

Fig. 12. Comparison of the lift-up distance correlation and measured data (● denotes the data and the 3-D surface represents the correlation $2L/D_{wf} = -1.150 + 12.15/\ln(Ra) + 0.0055Re^{0.5}\ln(Re)$).

4. Concluding remarks

The combined buoyancy and inertia driven vortex flow pattern associated with a round air jet impinging onto a heated disk confined in a vertical cylindrical chamber, simulating the flow in a single-wafer RTP processor, has been investigated by a detailed flow visualization in the present study. Effects of the inlet gas flow rate, temperature difference between the wafer and air jet, and chamber pressure on the resulting recirculating flow pattern were inspected in detail. The major results obtained here can be briefly summarized in the following:

(1) The typical flow pattern resulting from the air jet impinging onto a heated copper plate in the processing chamber is in the form of two axisymmetric circular vortex rolls having deformed cross-sections.
(2) A rise in the gas flow rate causes the inner vortex roll to become substantially larger and the outer vortex roll becomes correspondingly smaller.
(3) The higher buoyancy associated with the larger temperature difference between the wafer and air jet results in a slightly smaller inner roll and hence a larger outer roll.
(4) At a higher chamber pressure the Rayleigh number of the flow is higher, resulting a slightly smaller inner roll and hence a larger outer roll.
(5) The temporal state of the gas flow is delineated by a flow regime map and an empirical correlation, which indicate that the recirculating flow is steady at low buoyancy and inertia. At intermediate buoyancy and inertia time periodic flow prevails. The flow is chaotic in time at high buoyancy and inertia.

Acknowledgements

The financial support of this study by the engineering division of National Science Council of Taiwan, ROC through the contract NSC 89-2212-E-009-037 is greatly appreciated.

References

[1] S. Polat, B. Huang, A.S. Mujumdar, W.J.M. Douglas, Numerical flow and heat transfer under impinging jets: a review, in: C.L. Tien, T.C. Chawla (Eds.), Annular Review of Numerical Fluid Mechanics and Heat Transfer, vol. 2, Hemisphere, Washington, DC, 1989, pp. 157–197.
[2] G.B. Stringfellow, Organometallic Vapor Phase Epitaxy: Theory and Practice, Academic Press, San Diego, 1989 (Chapter 5).
[3] S.A. Campbell, The Science and Engineering of Microelectronic Fabrication, Oxford University Press, New York, 1996 (Chapter 6).
[4] R. Gardon, J.C. Akfirat, The role of turbulence in determining the heat-transfer characteristics of impinging jets, Int. J. Heat Mass Transfer 8 (1965) 1261–1272.
[5] R. Gardon, J.C. Akfirat, Heat transfer characteristics of impinging two-dimensional air jets, ASME Trans. C; J. Heat Transfer (1966) 101–108.
[6] M.T. Scholtz, O. Trass, Mass transfer in a nonuniform impinging jet, AIChE J. 16 (1970) 82–96.
[7] E.M. Sparrow, T.C. Wong, Impingment transfer coefficients due to initially laminar slot jets, Int. J. Heat Mass Transfer 18 (1975) 597–605.
[8] J.H. Masliyah, T.T. Nguyen, Mass transfer due to an impinging slot jet, Int. J. Heat Mass Transfer 22 (1979) 237–244.
[9] P. Hrycak, Heat transfer from round impinging jets to a flat plate, Int. J. Heat Mass Transfer 26 (1981) 1857–1865.
[10] İ.B. Özdermir, J.H. Whitelaw, Impingement of an axisymmetric jet on unheated and heated flat plates, J. Fluid Mech. 240 (1992) 503–532.
[11] T. Liu, J.P. Sullivan, Heat transfer and flow structures in an excited circular impinging jet, Int. J. Heat Mass Transfer 39 (1996) 3695–3706.
[12] A.R.P. Heiningen, A.S. Mujumdar, W.J.M. Douglas, Numerical prediction of the flow field and impingement heat transfer caused by a laminar slot jet, ASME Trans. C; J. Heat Transfer 98 (1976) 654–658.
[13] N.R. Saad, W.J.M. Douglas, A.S. Mujumdar, Prediction of heat transfer under an axisymmetric laminar impinging jet, Int. Eng. Chem. Fundam. 16 (1977) 148–154.
[14] H.S. Law, J.H. Masliyah, Mass transfer due to a confined laminar impinging axisymmetric jet, Int. Eng. Chem. Fundam. 23 (1984) 446–454.
[15] S.M. Hosseinalipour, A.S. Mujumdar, Comparative evaluation of different turbulence models for confined impinging and opposing jet flows, Numer. Heat Transfer, Part A 28 (1995) 647–666.
[16] G.K. Morris, S.V. Garimella, Orifice and impingement flow fields in confined jet impingement, ASME Trans. C; J. Heat Transfer 120 (1998) 68–72.
[17] Z.H. Lin, Y.J. Chou, Y.H. Hung, Heat transfer behaviors of a confined slot jet impingement, Int. J. Heat Mass Transfer 40 (1997) 1095–1107.
[18] D.L. Besserman, F.P. Incropera, S. Ramadhyani, Experimental study of heat transfer from a discrete source to a circular liquis jet with annular collection of the spent fluid, Exp. Heat Transfer 4 (1991) 41–57.
[19] D.L. Besserman, S. Ramadhyani, F.P. Incropera, Numerical simulation of laminar flow and heat transfer for liquid jet impingement cooling of a circular heat source with annular collection of the spent fluid, Numer. Heat Transfer, Part A 20 (1991) 263–278.
[20] R. Viskanta, Heat transfer to impinging isothermal gas and flame jets, Exp. Therm. Fluid Sci. 6 (1993) 111–134.
[21] K. Jambunathan, E. Lai, M.A. Moss, B.L. Button, A review of heat transfer data for single circular jet impingement, Int. J. Heat Fluid Flow 13 (1992) 106–115.
[22] G. Wahl, Hydrodynamic description of CVD processes, Thin Solid Films 40 (1977) 13–26.
[23] Y. Kusumoto, T. Hayashi, S. Komiya, Numerical analysis of the transfer phenomena in MOCVD process, Jpn J. Appl. Phys. 24 (1985) 620–625.

[24] D.I. Fotiads, S. Kieda, Transport phenomena in vertical reactors for metal organic vapor phase epitaxy, J. Cryst. Growth 102 (1990) 441–470.
[25] A.H. Dilawari, J. Szekely, A mathematical representation of a modified stagnation flow reactor for MOCVD application, J. Cryst. Growth 108 (1991) 491–498.
[26] C.R. Biber, C.A. Wang, S. Motakef, Flow regime map and deposition rate in vertical rotating-disk OMVPE reactor, J. Cryst. Growth 123 (1992) 545–554.
[27] P.N. Gadgil, Optimization of a stagnation point flow reactor design for metal organic chemical vapor deposition by flow visualization, J. Cryst. Growth 134 (1993) 302–312.
[28] C.R. Kleijn, T.H. van der Meer, C.J. Hoogendoorn, A mathematical model for LPCVD in a single wafer reactor, J. Electrochem. Soc. 136 (1989) 3423–3433.
[29] S. Chatterjee, I. Trachtenberg, T.F. Edgar, Mathematical modeling of a single-wafer RTP thermal reactor, J. Electrochem. Soc. 139 (1992) 3682–3689.
[30] P.N. Gadgil, Single wafer processing in stagnation point flow CVD reactor: prospects, constrains and reactor design, J. Electron. Mater. 22 (1993) 171–177.
[31] S.J. Kline, F.A. McClintock, Describing uncertainties in single-sample experiment, Mech. Eng. 75 (1953) 3–8.
[32] M.L. Hitchman, K.F. Jensen, Chemical Vapor Deposition (Principle and Application), Academic Press, San Diego, 1993 (Chapter 2).